Journal of Electronics, Electromedical Engineering, and Medical Informatics
Homepage: jeeemi.org; Vol. 8, No. 2, April 2026, pp: 622-637 e-ISSN: 2656-8632

RESEARCH ARTICLE OPEN ACCESS

Topographic EEG Power Mapping and Machine Learning-Based Seizure Detection Using Real and Synthetic SSIM-MSE Features

Ghansyamkumar Rathod and Hardik Modi

Department of Electronics and Communication, Chandubhai S Patel Institute of Technology, Charotar University of Science and Technology, Gujarat, India

Corresponding author: Ghansyamkumar Rathod (e-mail: 17drec016@charusat.edu.in), **Author(s) Email**: Hardik Modi (e-mail:hardikmodi.ec@charusat.ac.in)

Abstract **The neural activities of the brain can show abnormalities and misfiring due to seizures. The ionic activity of the brain can be converted into electrical activity, which can be observed on the human scalp using electroencephalography (EEG). The spatial patterns of brain activity can be analyzed using topographic maps generated from EEG signals. In this study, topographic power maps with seizure and normal states of the brain were generated, and the features of the image were named structural similarity index (SSIM) and mean square error (MSE). The data utilized in this study were obtained from a publicly available dataset from the Children's Hospital Boston (CHB) in association with the Massachusetts Institute of Technology (MIT). Topographic images of the bipolar montages showed a clear difference between seizure and non-seizure brain states, along with the affected areas of the brain regions. Synthetic Features were generated to mimic real data for training the ML models. The major tested machine learning models, gradient boosting, decision tree, and k-nearest neighbors, provided the highest accuracy of 99.34% and an F-score of 0.996 when evaluated using real and generated data. The generalizability of the model was confirmed using 5-fold cross-validation. Overall, this study provides an EEG power-based topographic power image generation along with reliable feature extraction to train ML models for detecting epileptic seizures. The proposed methodology not only enhances the interpretability of EEG spatial patterns but also offers potential for integration into biomedical wearable devices for real-time seizure monitoring and intervention, along with the identification of the type of seizure.**

Keywords **Topographic power map, Epilepsy, Electroencephalogram, Machine Learning**

I. Introduction

Globally, more than 50 million people are affected by epilepsy, a brain-related disorder that occurs because of the misfiring of neurons. One of the most reliable tools for detecting epilepsy is the method known as electroencephalography (EEG), a non-invasive method that converts the ionic activities of neurons into electrical signals and has a high temporal resolution [1], [2], [3]. Traditional methods for epilepsy detection based on EEG emphasize signal features related to frequency, wavelet, amplitude, and entropy. In this study, raw EEG signals were used to develop topographic maps, and image features were used to train the ML classifiers. The accuracy achieved in the range of 98-99% on public datasets in this study [4], [5].

In our study, we proposed a method in which topographic maps were generated based on the power distribution of the scalp. Furthermore, image features, namely the Structural Similarity Index Measure (SSIM) and Mean Square Error (MSE), were identified, which are widely used in image processing to capture both structural and pixel-level variations [6], [7]. Generative adversarial networks (GANs) have been explored for synthesizing EEG-like data generation but due to limited real datasets, we used feature spaced augmentation which is discussed in detail in method section. This feature provides an interpretable and computationally efficient method for distinguishing brain states, unlike many deep-learning-based black-box models [8], [9].

Topographic maps of EEG signals can be developed using this study, and the power distribution of each channel can be mapped in the image. Topographic images are used by medical experts to obtain a clear understanding of the areas affected by epilepsy. Our research is important for filling the gap in obtaining spatial information on how seizures propagate across the brain regions. This can help classify the seizure type and its severity [10], [11].

The normal and ictal signals are labeled with time stamps in the CHB-MIT dataset. From this dataset, 20-s fixed-length epochs were segmented to ensure a

Manuscript received 30 January 2026; Revised 20 March 2026; Accepted 2 April 2026; Available online 10 April 2026
Digital Object Identifier (**DOI**): https://doi.org/10.35882/jeeemi.v8i2.1515

reliable estimation of the channel-wise power. The sampling frequency of the utilized datasets is 256 Hz; that is, each epoch contains 5120 samples, providing sufficient statistical stability for power computation. To extract robust features, longer epochs are recommended because the variance of the mean squared amplitude estimates decreases inversely with the sample size. Furthermore, previous studies on seizure detection support a longer sample size, commonly between 10 and 30 s, to balance temporal resolution and feature reliability.

Channel-wise EEG power was computed as the mean squared amplitude over 20-s epochs. Each bipolar channel was assigned an approximate scalp coordinate, and spatial interpolation was applied to reconstruct the continuous scalp-power distribution. Cubic interpolation was used to generate smooth topographic power maps for the normal and ictal states using a common color scale, which enabled a direct visual comparison of spatial power patterns [12].

The Structural Similarity Index (SSIM) and Mean Squared Error (MSE) were computed between normal and ictal EEG topographic power maps. MSE quantifies absolute pixel-wise intensity differences, whereas SSIM assesses structural similarity by evaluating the luminance, contrast, and spatial organization. Additionally, SSIM difference maps were generated to visualize the localized scalp regions exhibiting maximal differences between the normal and seizure states [7].

The publicly available epilepsy datasets by CHB-MIT with appropriate labeling of epilepsy epochs were preprocessed by applying appropriate filters to remove power line noise, motion artifacts, baseline wandering, eye blinking noise, and ECG noise [13], [14]. The preidentified epochs of 20 seconds of normal and epileptic signals were used to generate topographic maps. This is shown in the block diagram in Fig.1. As shown in Fig. 1, the SSIM and MSE features were used to train the machine learning model, along with the generation of synthetic data for the best performance of the ML models. Finally, the performance of all models was compared to obtain better results for epilepsy detection [15], [16].

Most studies use seizure detection methods based on time-domain statistics, frequency-domain power features, or deep learning models that are directly applied to multichannel EEG signals. In the proposed approach, we first convert EEG channel-wise power into spatial scalp topographic maps and then apply image similarity metrics. The matrices used in our study are the structural similarity index measure (SSIM) and mean squared error (MSE), to quantify spatial differences between normal and ictal states. The conversion of signal space to image space offers a interpretable spatial analysis of seizure-induced power redistribution. Deep neural networks require large training datasets and extensive computational resources; in contrast, the proposed method supports a lightweight, explainable, and computationally efficient alternative for seizure characterization.

The main contribution of the proposed work is based on image-based feature extraction and identifying seizure occurrence based on lightweight machine learning models, which require low computational power. The spatial variations between normal and ictal state is plotted on an image can help detect seizure types, which can be useful for developing biomedical application-based hardware development.

II. Method

A. Preprocessing of the Raw Data

The preprocessing of raw data is crucial for removing noise. The publicly available datasets of patients with epilepsy were provided by the CHB-MIT on the PhysioNet repository and can be downloaded from the online link https://physionet.org/content/chbmit/1.0.0/. The EEG recordings with bipolar montages were further processed to obtain filtered data. The methods necessary to filter the data are discussed further [17].

A band-pass Butterworth filter was used for preprocessing, limiting certain frequencies to be removed, which were caused by noise, such as the movement of patients, power line noise, eye blinking, respiration, and heartbeat [18], [19]. The normalized cutoff frequencies can be represented by the following Eq. (1) [18].

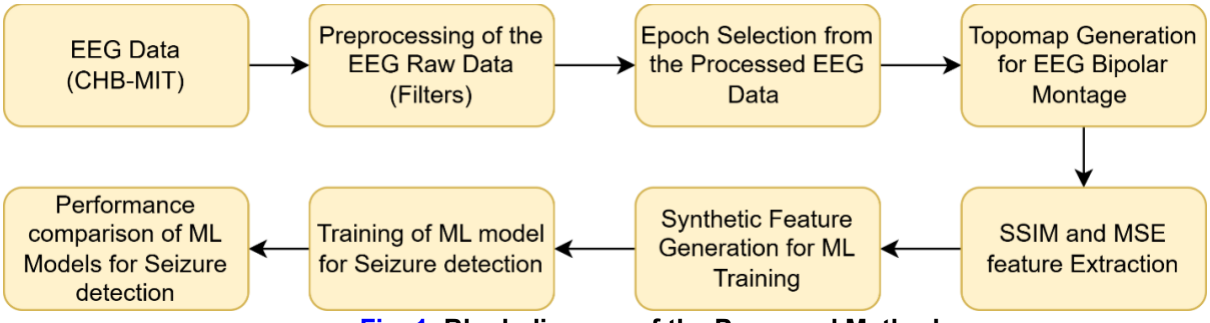

Fig. 1. Block diagram of the Proposed Method

Manuscript received 30 January 2026; Revised 20 March 2026; Accepted 2 April 2026; Available online 10 April 2026
Digital Object Identifier (**DOI**): https://doi.org/10.35882/jeeemi.v8i2.1515

$$\omega_{low} = \frac{f_{low}}{\frac{f_s}{2}}, \omega_{high} = \frac{f_{high}}{\frac{f_s}{2}} \quad (1)$$

Where, the lower cut off frequency f_{low} = 0.5 Hz and the higher cut off frequency f_{high}= 40 Hz with a sampling rate f_s = 256 Hz. The transfer function of a 4th order Butterworth filter can be represented by Eq. (2)[18].

$$H(z) = \frac{b_0 + b_1 z^{-1} + \ldots + b_4 z^{-4}}{a_0 + a_1 z^{-1} + \ldots + a_4 z^{-4}} \quad (2)$$

The filter takes the input signal and combines delayed versions of it. Here, z^{-1}, z^{-2},meaning previous samples. The numerator coefficient b_k control the feedback forward part and denominator coefficient a_k controls feedback enabling sharper frequency behavior. The time domain difference is shown in Eq. (3) [18].

$$y[n] = \left(\frac{1}{a_0}\right)(b_0 x[n] + b_1 x[n-1] + b_2 x[n-2] + b_3 x[n-3] + b_4 x[n-4]\ a_1 y[n-1] - a_2 y[n-2] - a_3 y[n-3] - a_4 y[n-4]) \quad (3)$$

where, $x[n]$ is the input EEG, $y[n]$ is filtered EEG and a_k, b_k are filter coefficients from Butterworth design. To get the $y_f[n]$, apply forward filter $H(z)$ and to get $y[n]$ back, apply reverse the signal and apply filter again. This process is necessary to get no phase distortion and it is important as far as EEG signal wave shape and timing matters. The frequency domain formula of the Butterworth filter can be represented by Eq. (4) [18], [19].

$$|H(j\omega)|^2 = \frac{1}{1+\left(\frac{\omega}{\omega_c}\right)^{2n}} \quad (4)$$

where, ω is the frequency that we are analyzing, ω_c is cut off frequency, and n is the filter order. The 4th-order Butterworth band-pass filter was used EEG preprocessing with cutoff frequencies of 0.5 Hz and 40 Hz. A bilinear transformation was used to obtain a digital implementation, resulting in a rational transfer function in the z-domain. To eliminate the phase distortion, zero-phase filtering was applied using forward-backward filtering.

Z-score normalization was performed to normalize the smoothed EEG signal. The baseline bias can be removed using the mean value computation, whereas the signal variability can be quantified using the standard deviation [20]. To normalize each sample, the mean was subtracted and divided by the standard deviation. To ensure numerical stability, when the standard deviation was below 10^{-5} , it was set to unity to avoid division by near-zero values. This normalization step ensured amplitude-invariant analysis across subjects and channels.

B. Topomap Generation

Channel-wise EEG power was computed as the mean squared amplitude of the signal over each epoch. The channel wise power computation can be done using Eq. (5) [34] to generate topographic power map.

$$P_c = \frac{1}{N}\sum_{n=0}^{N-1} x_c^2[n] \quad (5)$$

where, P_c is the average power of channel c in μV^2, $x_c[n]$ is EEG amplitude at sample n and N is the total number of samples in epoch. Normally, the power represents signal energy. Seizure activity is characterized by increased synchronization and higher amplitude oscillations. Hence, ictal epochs show higher power than the normal epochs. This equation provides a single scalar value per channel, which is ideal for scalp mapping and it's also provides a stable estimate of signal energy suitable for spatial power mapping.

To construct continuous scalp topographic maps from discrete electrode power values, cubic interpolation was applied. Each bipolar channel is assigned 2-D scalp coordinates x_c and y_c, which represent the approximate scalp location. The coordinates were normalized to a head-centered Cartesian coordinate system. The CHB-MIT data are bipolar; therefore, each bipolar pair is treated as spatially localized. This approximation is commonly used for visual comparison, rather than inverse-source localization [21], [22]. For above mentioned coordinates, the continuous power function can be represented by Eq. (6) [34].

$$\hat{P}(x,y) = \sum_{c=1}^{C} \omega_c(x,y) P_c \quad (6)$$

where, C is the number of channels and $\omega_c(x,y)$ are cubic interpolation basis weights computed from neighboring electrodes, which ensure smooth spatial transitions. These interpolations reconstruct smooth topographic distributions. The color scales of the image also need to be normalized for ictal and normal states to ensure accurate comparisons of each topographic image generated. [23] The map generated topographic map for the subject 1 and subject 2, considering the criteria explained in this section is shown in Fig. 2. Where, Fig 2(a) and Fig 2(c) shows a topographic maps of normal brain state and Fig 2(b) and Fig 2(d) shows a map of seizure brain state.

C. Image Features MSE and SSIM

The mean square error (MSE) is a common metric used to quantify the difference between two images, such as the original and processed images, by averaging the squared pixel differences. In our research, we utilized two images, which are topographic power maps of the normal and seizure states. The MSE can be calculated using Eq. (7) [24].

$$MSE = \frac{1}{MN}\sum_{i=1}^{M}\sum_{j=1}^{N}(I_N(i,j) - I_S(i,j))^2 \quad (7)$$

where, M, N represent image height and width, $I_N(i,j)$ is pixel at position (i,j) in normal map and $I_S(i,j)$ is pixel at position (i,j) in seizure map. $(I_N(i,j) - I_S(i,j))^2$ shows the squared pixel-wise difference, and shows the average squared intensity difference. The MSE measures the absolute pixel-wise difference, which is sensitive to power magnitude changes and color or

Manuscript received 30 January 2026; Revised 20 March 2026; Accepted 2 April 2026; Available online 10 April 2026
Digital Object Identifier (**DOI**): https://doi.org/10.35882/jeeemi.v8i2.1515

intensity shifts. Seizure maps usually show high-power regions, which lead to higher MSE [6].

Another feature SSIM known the Structural Similarity Index Measure (SSIM), is a metric that quantifies the visual similarity between two images by comparing the luminance or brightness, contrast, and structure. In the proposed method, the SSIM can be represented by Eq. (8) [6].

$$SSIM(I_N, I_S) = \frac{(2\mu_N\mu_S+C_1)(2\sigma_{NS}+C_2)}{(\mu_N^2+\mu_S^2+C_1)(\sigma_N^2+\sigma_S^2+C_2)} \quad (8)$$

where, μ_N, μ_S are mean of Normal and Seizure images used for luminance calculation as shown in Eq. (9) and Eq. (10). Whereas the σ_N^2, σ_S^2 are variance of Normal and Seizure images, which are used to measure spatial contrast indicating power spread across scalp as shown in Eq. (11) and Eq. (12) [36].

$$\mu_N = \frac{1}{MN}\sum I_N(i,j) \quad (9)$$

$$\mu_S = \frac{1}{MN}\sum I_S(i,j) \quad (10)$$

$$\sigma_N^2 = \frac{1}{MN}\sum (I_N - \mu_N)^2 \quad (11)$$

$$\sigma_S^2 = \frac{1}{MN}\sum (I_S - \mu_S)^2 \quad (12)$$

Covariance structure refers to how pixel values are related to each other, capturing spatial dependencies such as edges and textures and transformations such as scaling and rotation. It can be represented by Eq. (13) [36].

$$\sigma_{NS} = \frac{1}{MN}\sum (I_N - \mu_N)(I_S - \mu_S) \quad (13)$$

It measures structural similarity and captures whether high/low power regions occur at the same scalp locations. Publicly available datasets from Children's Hospital Boston in association with the Massachusetts Institute of Technology were used with synthetic samples generated in SSIM and MSE feature spaces. Synthetic data generation was used to address class imbalance and test robustness without relying solely on large-scale real-world recordings. Real and synthetic data were merged, and the feature matrix for the

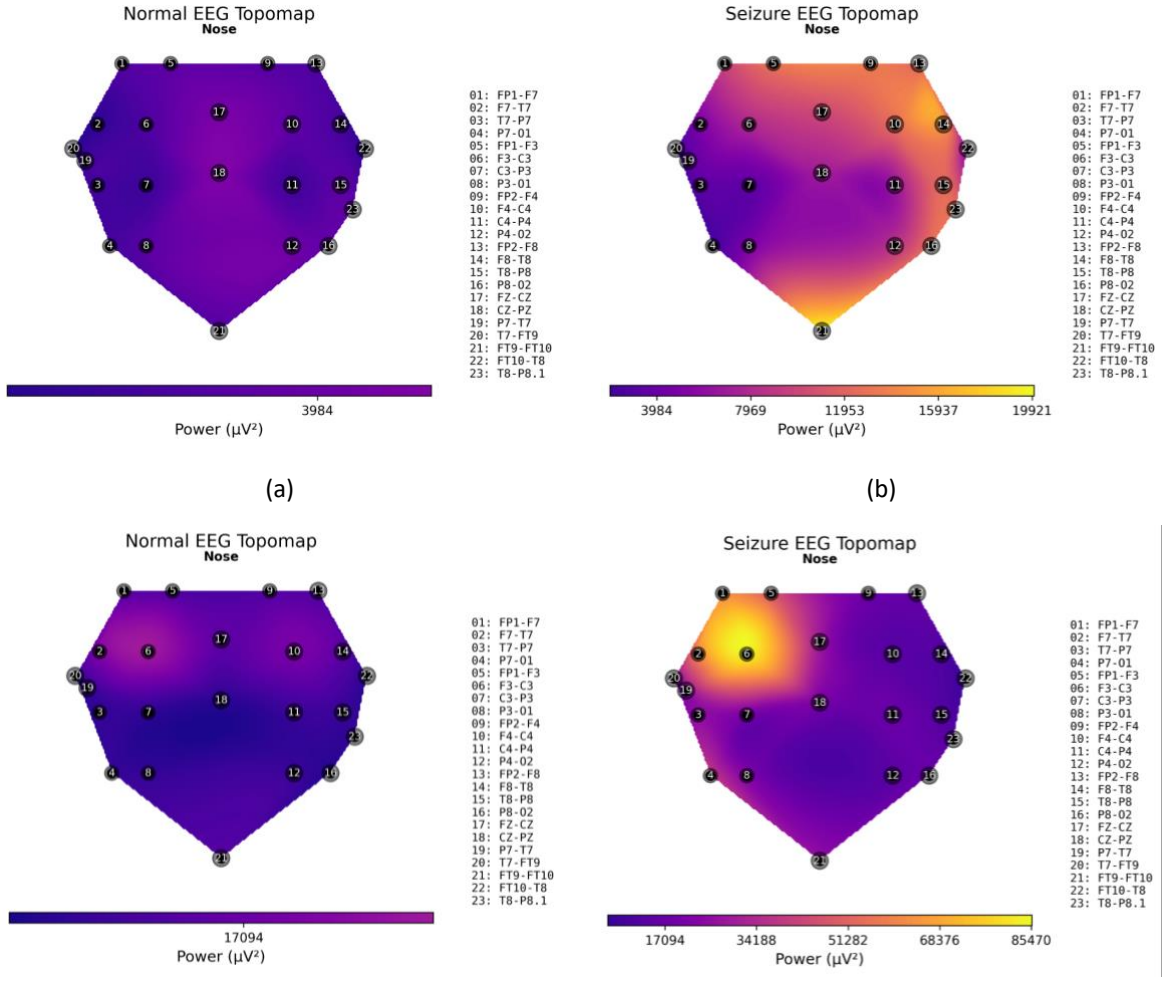

Fig. 2. Topographic Map of Power Distribution for the brain state of (a) Normal (b) Seizure for subject no. 1 and (c) Normal (d) Seizure for Subject no. 2

Manuscript received 30 January 2026; Revised 20 March 2026; Accepted 2 April 2026; Available online 10 April 2026
Digital Object Identifier (**DOI**): https://doi.org/10.35882/jeeemi.v8i2.1515

machine learning algorithm can be represented by Eq. (14) [25].

$$x_i = \begin{bmatrix} SSIM_i \\ MSE_i \end{bmatrix}, y_i \in \{0,1\} \quad (14)$$

where, $SSIM_i$ is structural similarity between normal and ictal EEG topographic maps, MSE_i Mean squared error between the same maps, $y_i = 0$ shows seizure normal or mild effect while $y_i = 1$ shows moderate or severe effect.

D. Synthetic Data for Scaling Model Development

The CHB-MIT datasets have a limited number of subjects, and to address this issue, we generated synthetic datasets mimicking the statistical distributions of the SSIM and MSE values from real EEG topomaps. This supports the effective training and testing of ML models. Minor variations are possible owing to the use of synthetic datasets; however, the models remain robust, particularly in maintaining high recall. For the selected subjects, the features SSIM and MSE data can be represented by Eq. (15) [25].

$$D_{real} = \{(SSIM_i, MSE_i)\}_{i=1}^{6} \quad (15)$$

Synthetic data generation is performed to obtain the best results while training the machine learning models. The synthetic data with the necessary label along with severity assignment can be represented by the interpretation shown in the distribution given in Table 1.

Table 1. Variable Explanation

Variable	Meaning
Severity	Proxy indicator of seizure impact (Mild / Moderate / Severe)
Label	Binary class: 0 = Normal-like, 1 = Seizure
Thresholds	Derived from observed SSIM–MSE separation in real data

The synthetic data and real data can be combined to train the machine learning model. The combined data can be represented by Eq. (19) [26].

$$D_{synthetic} = \{(SSIM_k, MSE_k, \text{Severity}_k, \text{Label}_k)\}_{k=1}^{500} \quad (19)$$

The real and synthetic data are merged for the machine learning model as shown in Eq. (20) [26].

$$D_{combined} = D_{real} \cup D_{synthetic} \quad (20)$$

To reduce the limitations of the small real region features, large-scale synthetic feature samples were generated in the SSIM-MSE feature space using uniform distributions restricted within physiologically

Table 2. Comparison of features for appropriate interpretation

Subject No	SSIM	MSE(μV²)	Interpretation
1	0.8833	57.00	Moderate Structural change, Strong Power Change
2	0.9327	46.57	Structurally Similar, Low Power Change
3	0.6974	50.78	Significant structural difference, Moderate Power Change
4	0.8232	58.01	Moderate Structural change, Strong Power Change
5	0.9438	52.83	Structurally Similar, Moderate Power Change
6	0.8611	51.51	Moderate Structural change, Moderate Power Change

In proposed method, the synthetic data were generated based on the real feature values [25]. For each synthetic subject $k = 1,2,3,4, \ldots \ldots 500$: The features can be uniformly distributed as shown in the Eq. (16) [25] and Eq. (17) [25].

$$SSIM_k \sim U(0.65, 0.95) \quad (16)$$

$$MSE_k \sim U(40, 70) \quad (17)$$

where, $SSIM_k$ is structural similarity between normal and ictal topographic maps, MSE_k is mean square error between normal and ictal topographic maps, $U(a, b)$ is continuous uniform distribution in range [a, b] and $n = 500$ which is number of synthetic samples generated. For each synthetic sample, the severity and label can be shown as per Eq. (18) [26].

$$(Severity_k, Label_k) = \begin{cases} (Mild, 0), & if\ SSIM_k \geq 0.90\ \Lambda\ MSE_k < 50 \\ (Moderate, 1), & if SSIM_k \geq 0.80\ \Lambda\ MSE_k < 50 \\ (Severe, 1), & otherwise \end{cases} \quad (18)$$

along with a reduction in overfitting. The outline of the probable ranges. The rule-based decision function was derived from real EEG observations and was employed to assign severity levels along with binary labels. This synthetic dataset was combined with real data to enhance the classifier robustness and generalization, feature distribution, along with the class balance, can be maintained by generating synthetic data. By observing the real data patterns, the labels were assigned using rule-based thresholds. Recent studies have shown that if synthetic biomedical data are molded carefully, they can enhance model robustness and reduce the risk of overfitting [26], [27].

E. Machine Learning Performance and Interpretability

The two datasets were combined to train the machine learning algorithms. The feature vector to train these algorithms is as represented in Eq. (21) [25].

$$x_i = \begin{bmatrix} SSIM_i \\ MSE_i \end{bmatrix}, y_i \in \{0,1\} \quad (21)$$

Manuscript received 30 January 2026; Revised 20 March 2026; Accepted 2 April 2026; Available online 10 April 2026
Digital Object Identifier (**DOI**): https://doi.org/10.35882/jeeemi.v8i2.1515

where, the value of y_i shows the severity of the seizure. Initially, the feature normalization is done. The normalized feature can be represented as follows in Eq. (22) [28]. This is required because SSIM and MSE have different numerical scales. Standardization prevents the dominance of high-magnitude features.

$$z_{ij} = \frac{x_{ij} - \mu_j}{\sigma_j} \quad (22)$$

where, x_{ij} value of feature j for sample i. μ_j is mean of feature j over training data. σ_j is the standard deviation of feature j.The dataset is split into 70% training and 30% of test data. The features SSIM and MSE, which were derived from the EEG topographic power maps, can be used to perform machine learning classification [28]. The most famous classifiers, namely Logistic Regression, Support Vector Machine, Random Forest, Gradient Boosting etc., were evaluated. All features were standardized, and the standard method of train-test and splitting was applied. The performance of the ML models was evaluated based on accuracy, precision, recall, F1-score, ROC-AUC, and 5-fold cross-validation. A dummy classifier was used as a baseline to validate the performance improvements [2]. Machine learning model decision boundaries can be defined by Eq. 23 [29] for logistic regression model.

$$P(y = 1|x) = \frac{1}{1+e^{-(w_0+w_1x_1+w_2x_2)}} \quad (23)$$

where, y is the target class label (0=Normal, 1 = seizure), x is the feature vector of the sample, x_1 is the first feature (SSIM) and x_2 is the second feature (MSE), $w_o$is the intercept term of the classifier, $w_1$is the weight assign to SSIM feature and w_2 is weight assign to MSE feature. The predicted class label is determining by Eq. 24 [29].

$$\hat{y} = \begin{cases} 1, if\ P(y = 1|x) \geq 0.5 \\ 0, if\ P(y = 1|x) < 0.5 \end{cases} \quad (24)$$

where, $\hat{y}$ is the predicted class label and 0.5 is default probability threshold. A very simple model known as logistic regression performed well for the image feature-based approach applied by us, confirming that SSIM and MSE carry significant discriminative information. To show the results are stable, the confidence interval can be calculated using Eq. 25 [29].

$$CI_{95\%} = \bar{x} \pm 1.96 \cdot \frac{\sigma}{\sqrt{n}} \quad (25)$$

where, $\bar{x}$ is the mean matric (e.g., mean F1 from cross validation), σ is standard deviation and n is number of folds. By using the sigmoid function of the SSIM-MSE feature vector, the probability of seizure occurrence can be identify using the Logistic regression models. The weighted contributions of SSIM and MSE are used to compute a linear decision score by the classifier, and a logistic transformation is applied to estimate the class probability. Classification of samples is performed using the prediction of the probability by comparing the predefined threshold.

The classification performance of the ML models was supported by the combination of two features derived from the topographic power maps. Table 2 presents the results derived using this approach. We observed that the well-known classification models of machine learning, such as Gradient Boosting, K-Nearest Neighbors (KNN), and Decision Trees, achieved an accuracy of 99.3 %, a recall of 100 %, and a precision above 99 %. This supports the presence of seizure events without false negatives, which is a critical requirement for clinical diagnosis. ML models require large datasets and very high computational power for data processing [29], [30], [31], [32]. In our hypothesis,

Algorithm 1. Pseudocode for the applied method

```
FOR each subject x:
(1)  Load EDF → X_raw
(2)  Convert X_raw to CSV format
(3)  Pre-process:
     X_bp = bandpass(X_raw, f_low=0.5,
     f_high=40)
     X_smooth = SavitzkyGolay(S_bp)
     X_norm = Zscore(X_smooth)
(4)  Segment X_norm into 20-sec epochs
     (Normal, Ictal)
(5)  FOR each epoch e:
     FOR each channel c:
     P_c = mean(e[:,c]^2)        #for channel
     power
     END
     P_grid = cubic_interpolation(P_c,
     scalp_coords)
     save_topomap(P_grid)
     END
(6)  Load Normal map I_N and Ictal map I_X
(7)  MSE  = mean((I_N - I_X)^2)
(8)  SSIM = compute_SSIM(I_N, I_X)
(9)  Store feature vector X = [SSIM, MSE]
     END
(10) Generate synthetic features:
     SSIM_k ~ Uniform(a,b)
     MSE_k  ~ Uniform(c,d)
     Assign label using rule-based thresholds
(11) Combine real + synthetic dataset
(12) Standardize features
(13) Stratified split (70% train, 30% test)
(14) FOR each ML model in {LR, SVM, KNN,
     DT, RF, NB, GB}:
     Train model
     Predict test labels
     Compute Accuracy, F1, ROC-AUC
     Perform 5-fold cross-validation
     END
     RETURN best-performing classifier and
     metrics
```

Manuscript received 30 January 2026; Revised 20 March 2026; Accepted 2 April 2026; Available online 10 April 2026
Digital Object Identifier (**DOI**): https://doi.org/10.35882/jeeemi.v8i2.1515

we utilized lightweight, interpretable, and highly generalizable machine learning models to align with the recent growth in the Biomedical and AI sectors. The algorithm used to generate the necessary outputs from the available data sets is as shown in Algorithm 1.

III. Result

A. Feature Interpretation

The publicly available CHB-MIT datasets were converted to CSV files and preprocessed to remove common noises that affect biomedical potentials. Topographic maps of the CHB-MIT datasets were generated based on the power values added at specific locations on the scalp, highlighting the spatial color contrast from lower to higher values. The darker the color, the lower the power magnitude. Topographic maps with power densities on horizontal scale are shown in Fig. 2(a) (3984 μV^2) for similar subject (1 and 2) in normal brain state shown in Fig. 2(b) (19921 μV^2). Similarly for the seizure states shown in Fig. 2(c) (17094 μV^2) for normal state while Fig. 2(d) (85470 μV^2) for seizure state, power densities shown marginal differences. Topographic maps of the normal and seizure brain states were developed for similar participants and shown marginal changes in the values of power densities. The image features of the Structural Similarity Index (SSIM) and Mean Squared Error were acquired to differentiate between normal and seizure images for the subjects (1,2,3,4,and 5), as shown in Fig. 3 on the same color scale for values higher than 50 μV^2 of MSE gives higher impact of the seizure while near to and less than 50 μV^2 shows moderate effect of seizure. The lighter the color, the higher the magnitude of the power, as observed in the topographic maps of seizures compared with the normal maps. The severity of seizures can also be identified using machine-learning algorithms. The color range was standardized across all maps specific to participants to ensure visual consistency.

The SSIM and MSE values were calculated between each selected subject's (1,2,3,4,5 and 6) normal and seizure topographic maps, which yielded a compact and interpretable feature vector. A comparison of the SSIM and MSE values for a few subjects (1,2,3,4,5 and 6) is presented in Table 2.We can summarize the SSIM and MSE values for all selected subjects (1,2,3,4,5 and 6). Table 2 shows the values of both features, which were randomly selected from the subject's (1,2,3,4,5 and 6) datasets. The SSIM values ranged from 0.6974 to 0.9438, indicating varying degrees of similarity between the seizure and normal conditions. The MSE values varied from 46.57 to 58.01 μV^2, showing the average power difference across the topographic space, as shown in the Fig. 3.

B. Visual Validation

Topographic map for subjects (1 and 2) shown in Fig. 2(a) and Fig. 2(b), reveal prominent visual differences between the normal and seizure brain states. The spatial distribution became denser (light color) or shifted towards specific lobes in the seizure state, indicating regional hyperactivity. These visual patterns where SSIM for subject 1 is 0.8833 and MSE is 57 μV^2 and for suject 2 SSIM is 0.9327 and MSE is 46.57 μV^2 and so on derived from the real datasets correlate well, validating our choice of features for subjects (1,2,3,4 and 5), as shown in Fig. 3 and Table 2. Additionally, the topographic color intensity and contour variations were consistent across all subjects (1,2,3,4,5 and 6) when a unified color scale was applied, supporting the visual interpretation of seizure onset.

Table 3. The result summary of the Machine Learning Models

Model	Accuracy	F1-Score	ROC-AUC	CrossVal F1	Precision (Seizure)	Recall (Seizure)
Logistic Regression	0.9671	0.9827	0.9965	0.9885	0.9659	1.0
Random Forest	0.9868	0.9930	0.9972	0.9979	0.9861	1.0
SVM (RBF Kernel)	0.9868	0.9930	0.9993	0.9968	0.9861	1.0
K-Nearest Neighbors	0.9934	0.9965	1.0000	0.9978	0.9930	1.0
Decision Tree	0.9934	0.9965	0.9500	0.9989	0.9930	1.0
Naive Bayes	0.9803	0.9895	1.0000	0.9948	0.9793	1.0
Gradient Boosting	0.9934	0.9965	0.9500	0.9989	0.9930	1.0

C. Machine Learning Model Comparison

Seven commonly used Machine Learning models were trained on the combined dataset using a train-test split and 5-fold cross validation. Table 3 summarizes the model's (7 models) performance and the Fig.4 (a, b, c,

Manuscript received 30 January 2026; Revised 20 March 2026; Accepted 2 April 2026; Available online 10 April 2026
Digital Object Identifier (**DOI**): https://doi.org/10.35882/jeeemi.v8i2.1515

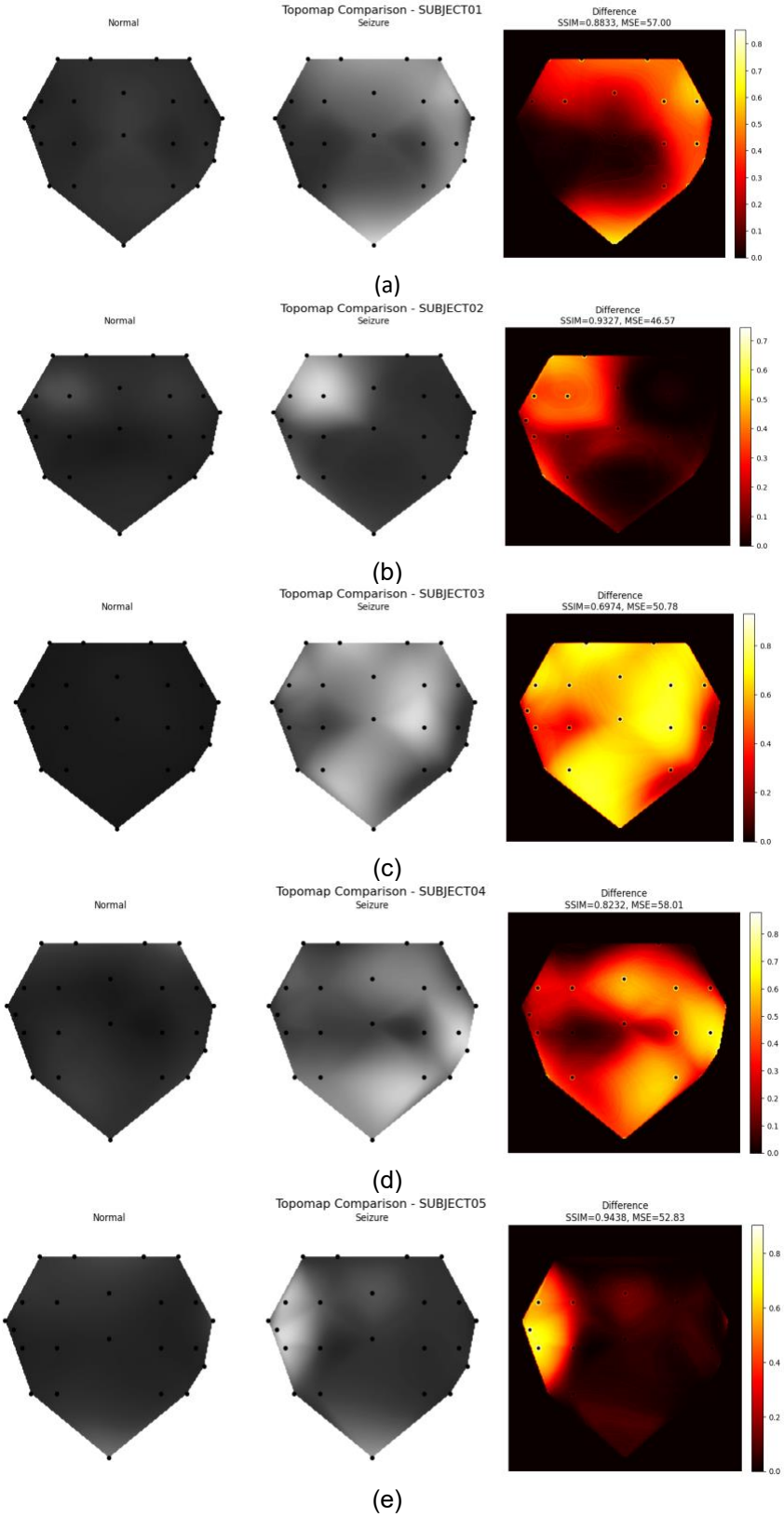

Fig. 3. The features SSIM and MSE extracted using topographic maps shown for the subject number (a) one (b) two (c) Three (d) Four, and (e) Five.

Manuscript received 30 January 2026; Revised 20 March 2026; Accepted 2 April 2026; Available online 10 April 2026
Digital Object Identifier (**DOI**): https://doi.org/10.35882/jeeemi.v8i2.1515

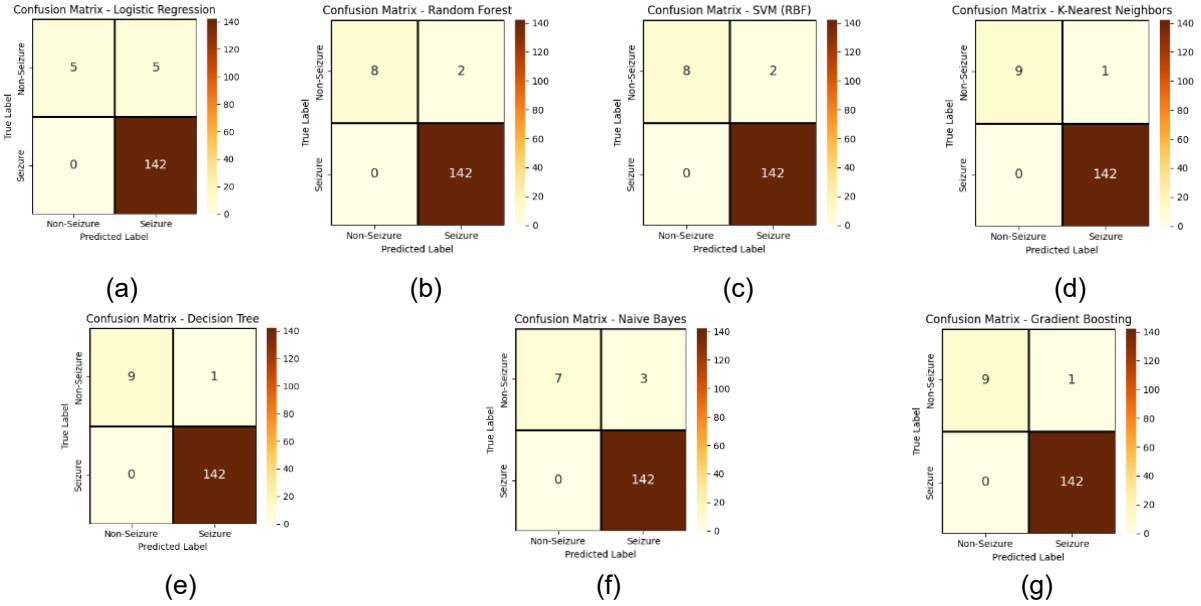

Fig. 4. The confusion matrices of ML Models (a) Logistic Regression (b) Random Forest (c) SVM (RBF Kernel) (d) K-Nearest Neighbors (e) Decision Tree (f) Naive Bayes (g) Gradient Boosting

ML models utilized for the proposed method. Various machine learning models were deployed, and based on their performances, accuracies of Gradient Boosting, Decision Tree, and KNN (99.34%) showed high performance with an F-1 score above 0.996, precision (99.30%) and perfect seizure recall (recall = 1). The ROC-AUC scores Gradient Boosting (0.95), Decision Tree (0.95) and KNN (1.0) indicate the separability between classes which are better compared to tested models. We performed 5-fold cross-validation and computed confidence intervals for the performance metrics to evaluate the robustness of the classification results. Ninety-five percent confidence intervals were estimated based on the mean and standard deviation of the F1-scores across folds, providing a statistical measure of model stability.

IV. Discussion

The innovative method uses image-based features to develop topographic power maps using EEG signals to detect seizure onset. The method applied here integrates spatial features that are used to train machine learning models. This method bridges a critical gap between the conventional signal-based seizure analysis.

A. EEG Data Acquisition and Preprocessing.

The data provided by the Children's Hospital, Boston, are in the EDF format and raw data with noise artifacts. These data are publicly available and consist of 23 channels with a sampling rate of 256 Hz. To process the data, the EDF format was converted to CSV format, and appropriate subjects (1,2,3,4,5 and 6), and epochs were selected according to the labels provided by the data provider for the ictal and normal states.

Twenty-second epochs of the normal and ictal states were acquired and preprocessed for further analysis. The 256 Hz sampling rate and 20-second-long epoch gives rich information of the onset. Preprocessing included band-pass filtering to remove higher-frequency noise, a notch filter (50 Hz) to eliminate power line interference, baseline correction, wavelet de-noising, de-trending, and normalization. These steps were applied to minimize motion artifacts, such as eye blinks, eye movements, and muscle activity, thereby ensuring clean and reliable signals for further analysis [16], [19], [20].

B. Topographic Power Map Generation

The preprocessed EEG epochs of the ictal and normal states were acquired, and the channel-wise power was computed using the mean square amplitude over time. To show the spatial distribution of power on a 2D map for the normal brain state, a topographic image was generated for subjects (1 and 2), as shown in Fig. 2(a) (~3984 μV^2) and Fig. 2(c) (~17094 μV^2) and values of power compared to colors can be verified on horizontal scales. Each bipolar channel was mapped to a coordinate on a simulated scalp, and the power values were interpolated across the grid using a cubic interpolation [33], [34]. The seizure state topographic maps for the subjects (1 and 2) are illustrated in Fig. 2(b) (~15937 μV^2) and Fig. 2(d) (~51282 μV^2). Where, the "Nose" label shows the frontal lobe orientation of the brain. The power values of normal and seizure state show marginal differences. The color scale was consistently used to highlight the differences between normal and seizure events. Channel names

Manuscript received 30 January 2026; Revised 20 March 2026; Accepted 2 April 2026; Available online 10 April 2026
Digital Object Identifier (**DOI**): https://doi.org/10.35882/jeeemi.v8i2.1515

were annotated with their corresponding scalp positions to retain visual interpretability, as shown on the right side of each topographic map in the Fig. 2 [34].

C. Effectiveness of Topographic EEG Mapping

The topographic map of subjects (1 and 2), as shown in Fig. 2, where normal and seizure events were highlighted, confirms the visible differences. The power maps show the spatial distribution of the signal power during seizures and the normal brain state, as shown in Fig 2 [34]. As shown in Fig. 2(b) and Fig. 2(d), specific regions of the brain, such as the temporal and occipital areas, showed elevated power levels (~19921 μV^2 and ~85470 μV^2), which aligned with the clinical expectations for focal epileptic activity. Conventional methods are based on frequency or time-domain analyses, which focus on signal behavior over time. Topographic maps offer a spatial perspective of neural dynamics. The main advantage of such topographic maps is that they aid visual interpretation and can enhance the neurologist's ability to localize epileptic foci, especially in datasets using bipolar montages, such as the CHB-MIT datasets [16].

The CHB-MIT dataset is acquired using a bipolar montage, wherein the potential difference between two electrodes is recorded from the scalp. Furthermore, channel-wise power calculations reflect the differential rather than absolute scalp activity. The expansion of the power expression indicates that bipolar power incorporates both individual electrode powers and their covariance terms. Compared with the unipolar montages, the direct spatial interpretability of the bipolar montage is reduced; however, the comparative analysis between normal and ictal states remains valid because both are evaluated under identical montage conditions. Topographic power maps for the selected subjects (1,2,3,4,5 and 6) were generated using an appropriate algorithm for bipolar montages, as shown in Fig. 2 and Fig. 3, where two electrodes were considered, and their average values were chosen as the amplitude of the signal at a specific channel location on the scalp. There are no ready algorithms or libraries available to generate topographic maps for bipolar montages of EEG, whereas for unipolar topographic map generation, there are many supporting GUI applications available to generate such topographic maps. The Minimum Norm Estimate (MNE) library supports in python language and EEG lab supports in MATLAB software programing simulators for unipolar EEG montages.

D. Significance of SSIM and MSE as Biomarkers

The calculation of SSIM and MSE considering the subjects (1,2,3,4,5 and 6) for normal and seizure topographic images can be used for quantitative comparison between spatial states. The SSIM values ranged from 0.69 to 0.94 and the MSE values from 46 to 58 across the subjects (1,2,3,4,5 and 6) as shown in Table 2, clearly showing a spatial change in power distribution during seizure onset. SSIM is more sensitive to luminance, contrast, and structure and can capture more holistically than pixel-based measurements. The MSE provides a magnitude-based performance comparison and complements the SSIM by offering a scale-based deviation [28], [35], [36]. Our methodology and approach are consistent with recent innovations that utilize image similarity techniques in EEG and medical imaging to detect cognitive or pathological changes. The use of two image-based features, namely SSIM and MSE, creates a compact and effective feature space for machine learning.

Two image-based features for subjects (1,2,3,4,5 and 6) were extracted to differentiate seizure (ictal or seizure) and non-seizure (normal) brain states from the EEG topographic power maps. The Mean Squared Error (MSE) and Structural Similarity Index Measure (SSIM). Mean Squared Error quantifies the average squared difference in the intensity of the pixels between two maps and shows how much the overall power distribution differs in magnitude. Lower magnitude values indicate higher similarity [28]. On the other hand, SSIM measures structural similarity by considering brightness, contrast, and spatial patterns. These reflect the intensity differences and changes in the arrangement of brain activity across regions. The MSE and SSIM features were chosen based on their interpretability, computational efficiency, and complementarity. MSE is effective in capturing intensity differences, whereas SSIM captures structural changes. The combined use of the MSE and SSIM can provide a comprehensive view of seizure-induced alterations. Moreover, these features are clinically relevant because they correspond directly to visual and spatial patterns in brain activity, making them easier to interpret than mathematical or deep learning features. Simplifying both the features, we can say that MSE (50 or above) tells us "How different the colors are" between two brain activity maps, and the SSIM (1 = identical images) tells us "How different the shapes and patterns are," allowing detection of both the magnitude and the structural nature of seizure activity [7], [28], [35], [36].

The similarity between two topographic images of the normal and ictal states is captured using the SSIM (1 = identical images) metric, which reflects the spatial redistribution of EEG power during seizure activity. Low SSIM values directly indicate stronger spatial disruption of cortical activity patterns. In contrast, MSE is used to quantify the magnitude of power differences between the two states. A higher MSE value corresponds to a stronger deviation from normal brain activity. By considering a combination of SSIM and MSE, it provides insight into both spatial and intensity-related changes associated with seizure events.

Manuscript received 30 January 2026; Revised 20 March 2026; Accepted 2 April 2026; Available online 10 April 2026
Digital Object Identifier (**DOI**): https://doi.org/10.35882/jeeemi.v8i2.1515

E. Synthetic Data Generation

EEG recordings often have limitations in seizure events compared to normal recordings in biomedical datasets. This imbalance can bias machine learning models considering the majority class and downgrade their ability to generalize for seizure detection. To improve the performance of such models, we introduced synthetic data generation [9]. We generated synthetic features in the SSIM-MSE feature space rather than creating artificial EEG waveforms. This approach ensured that the synthetic data were interpretable and consistent with real feature distributions. In particular, the statistical ranges of the SSIM (0.6 to 0.9) and MSE (42 to 70) values observed in the real dataset (mean and standard deviation) were used to guide the data generation. New feature pairs of SSIM and MSE were created by applying Gaussian sampling, while preventing duplication or leakage of the original data [7], [28], [35]. The augmentation strategy increases the diversity of the training samples and balances the datasets, which enhances the robustness of the classification. Moreover, when synthetic data are generated at the feature level, the complexity of the model can be reduced compared to waveform synthesis, which maintains a clear physiological interpretation of the data [9], [37].

F. Machine Learning Models

Real and synthetic datasets were prepared to train various machine learning models (LR, RF, SVM, KNN, DT, NB, GBM) to classify seizure and non-seizure epochs. Classifiers such as decision tree, gradient boosting, and k-nearest neighbors etc., were employed because of their complementary strengths [1], [2]. Each classification algorithm was trained using both real and synthetic features, ensuring balanced learning. The performance of each machine learning model was evaluated using multiple metrics. For Gradient Boost ML Model, the accuracy (99.34%), F-1 score (0.9965), recall (1), and precision (99.30%) metrics are shown and for the other models, same parameters help to understand the effectiveness of each model [1], [2]. To analyze the classification measures in detail, the confusion matrices (a, b, c, d, e, f and g) as shown in Fig. 4 were computed for all classifiers (LR, RF, SVM, KNN, DT, NB, GBM) based on the results of Table. 3. Insights into the seizure detection reliability and potential false alarm rates can be identified using these matrices, which provide true positive, true negative, false positive, and false negative values.

To confirm generalizability, a 5-fold cross-validation scheme was applied, where the datasets were divided into five equal parts, four of which were used to train the model, and one was used to check validation. These five parts, known as folds, are rotated until all folds are tested. The importance of this process is to reduce the overfitting of the model, and it allows for robust performance and fair comparison among classifiers. The approach used in this study not only tested the accuracy of the models but also rigorously tested the reliability of each model in the detection of seizure events, which is the core of this study. The use of subjects in the CHB-MIT datasets is limited; therefore, the statistical test did not reach conventional significance levels. Nevertheless, the SSIM and MSE features captured spatial differences between normal and ictal states, which were effectively implemented by ML (LR, RF, SVM, KNN, DT, NB, GBM) models trained on the augmented dataset. Deep learning-based methods require high computational resources and large datasets; in contrast, the proposed framework is computationally lightweight. The core processing steps are data preprocessing, power estimation, and image-based feature extraction, which require low computational complexity. Therefore, the proposed method can be efficiently implemented on standard computing systems, and specialized hardware, such as GPUs, is not required.

G. Comparison with Prior work

Recent innovations in seizure detection emphasize feature extraction methods along with deep learning architectures to improve accuracy and decrease latency. Wang et al. (2023) [38] used EEG signals to capture topological characteristics for persistent homology, and the results showed reduced latency and high event-based sensitivity. Another study done by Chung et al. (2024) [39] used a single-channel EEG signal to detect seizures using CNNs, where 97–100 % sensitivity was achieved along with a low false alarm rate. A study by Shen et al. (2024) [40] exploited short-time Fourier transform (STFT) spectrograms with GoogleNet CNN, where real-time seizure detection was achieved with an accuracy close to 98 %. Such deep learning approaches provide robust detection and often require substantial computational resources and large datasets for effective training. Feature selection and data augmentation-based research have been conducted by various authors. Ali et al. (2024) [41] evaluated overlooked aspects of the CHB-MIT dataset, showing that feature selection could yield efficient seizure detection using random forest where sensitivity remained limited (73-75%). Abou-Abbas et al. (2024) [42] highlighted the data scarcity through synthetic EEG generation with WGAN-GP, showing that augmentation improved LSTM-based detection performance with 5-8% on the TUSZ dataset. In prediction-based modeling, Zhu et al. (2024) [43] worked on multidimensional transformers with recurrent networks on the CHB-MIT and Bonn Datasets by acquiring a strong predictive performance with a sensitivity of 98.24 % and a specificity of 97.27 %.

Compared to the available research and literature review as shown in Table 4, our proposed methods

Manuscript received 30 January 2026; Revised 20 March 2026; Accepted 2 April 2026; Available online 10 April 2026
Digital Object Identifier (**DOI**): https://doi.org/10.35882/jeeemi.v8i2.1515

Table 4. Comparison of recent research with proposed method

Study	Dataset	Representation / Features	Model	Evaluation	Performance
Wang et al. (2023)[38]	CHB-MIT	Persistent homology (topological EEG features)	GoogLeNet CNN	Segment-based & event-based	Segment: Acc. 97.05%, Sens. 96.71%, Spec. 97.38%; Event: Sens. 100%, Latency: 1.22 s
Chung et al. (2024)[39]	CHB-MIT	Single-channel EEG, time–frequency	2D CNN	Patient-specific, event-level	Sensitivity: 97.05–100%, FAR: 0.22–0.40/hr, Latency: 2.1–3.4 s
Shen et al. (2024)[40]	CHB-MIT	EEG → STFT spectrograms	GoogLeNet CNN	Real-time framework	Accuracy ~98%, real-time feasibility
Ali et al. (2024)[41]	CHB-MIT	92 features (22 channels), reduced to 32	Random Forest + event post-processing	Cross-subject, 5-fold & LOO	Sensitivity: 72.63–75.34%
Abou-Abbas et al. (2024)[42]	TUSZ	Synthetic EEG via WGAN-GP	LSTM	Patient-wise GroupKFold	Accuracy ↑ by 5–8% with augmentation
Zhu et al. (2024)[43]	CHB-MIT, Bonn	Multidimensional STFT + time series	Transformer + LSTM/GRU	Cross-dataset validation	Sensitivity: 98.24%, Specificity: 97.27%
Proposed Method (2025)	CHB-MIT (20s epochs) + Synthetic data	Topographic EEG Power Maps → SSIM + MSE	ML (KNN, GBoost, DT, etc.)	Cross-validation	Accuracy: 99.34%, F1: 0.996, Seizure Recall: 100%

introduce a novel approach by generating topographic EEG power maps along with the extraction of image-based features named SSIM and MSE, which are used to train classification ML models (LR, RF, SVM, KNN, DT, NB, GBM). The study based on image-based feature extraction achieved an accuracy of 99.34 % along with perfect recall (one) for seizure events, outperforming several deep learning-based studies in terms of efficiency and generalizability. Additionally, the integration of synthetic data ensured robust training, despite limited feature availability. The interpretable and lightweight approaches are confirmed by the use of topographic power maps, which can match or exceed the performance of complex deep learning pipelines while being more suitable for resource-constrained biomedical wearable devices.

The proposed framework is based on a spatial analysis of EEG signals through topographic power maps of datasets from CHB-MIT seizure data of selected subjects (1,2,3,4,5 and 6). This approach effectively captures the spatial redistribution of cortical activity during a seizure, whereas the temporal features of EEG signals are not openly incorporated. Future work can be conducted based on temporal features, such as time-domain statistics, spectral features, or time–frequency representations, along with spatial topographic features, to provide a more suitable characterization of seizure activity.

When real-time EEG signals are recorded, motion artifacts, such as eye movements and muscle locomotion activities, are also often recorded. In addition, powerline noise and environmental noise can impact the actual EEG signals. Although the preprocessing steps applied in this study remove most of the aforementioned noise, more advanced artifact removal methods could further improve robustness.

Manuscript received 30 January 2026; Revised 20 March 2026; Accepted 2 April 2026; Available online 10 April 2026
Digital Object Identifier (**DOI**): https://doi.org/10.35882/jeeemi.v8i2.1515

Moreover, variability in seizure patterns across patients may also influence model generalization. Considering these challenges, the proposed framework offers computationally lightweight methods for machine learning and therefore has potential for real-time or near-real-time clinical monitoring applications. The features SSIM and MSE, derived from EEG topographic power maps, showed highly effective results while distinguishing brain states such as seizure and non-seizure. With the combination of real and synthetic data, the ML classifiers, namely, Gradient Boosting and KNN, achieved an F1-score above 0.996 with a seizure recall of 100 %. The most important rationale was to work on spatial EEG patterns using topographic power maps as a key biomarker for seizure detection. Generally, ML models used to classify seizures are frequency- and time-based. This method fills this gap by combining spatial visualization of topographic maps, similarity metrics, and interpretable machine learning.

H. Limitations of the Study

The datasets used in this study were limited to the CHB-MIT datasets. However, these datasets are very rich compared to the available datasets. The 20-second epochs of normal and ictal states were combined with synthetic data, and machine learning models were developed. In some cases, synthetic data may not capture all real-world variability. No temporal features, such as pre-ictal to ictal transition, were included. The use of Bi-polar montage can affect the spatial interpretation due to avoidance of temporal features. Validation was performed using cross-validation with limited sample size but not on external datasets.

V. Conclusion

This study is based on image feature extraction, where the SSIM and MSE image similarity features provide novel, efficient, and interpretable results for detecting seizures using topographic EEG power maps. The spatial differences in the EEG topographic power maps of normal and seizure states used in our study achieved high accuracy in classification, along with minimum feature complexity. The spatial representation of EEG signals using a topographic map for bipolar montage is crucial. Meaningful insights can be highlighted using image-based representations. Moreover, the use of synthetic data combined with real-time data can enhance model generalization and help evaluate multiple ML algorithms effectively. Among all the ML models, Gradient Boosting, KNN, and Decision Tree classifiers performed well with an F-1 score above 0.996 and perfect seizure recall. The proposed methodology provides support for an interpretable, unclouded, and computationally lightweight seizure detection framework that can be used in a clinical environment to make appropriate decisions. For future work, the method can be applied to multiple datasets along with the consideration of the temporal and spatial features to enhance the accuracy of the ML models.

Acknowledgment

The authors would like to thank the charotar university of science and technology for providing a computing facilities, feasible environment to work upon such findings on biomedical data.

Funding

This research did not receive any funding from any agencies or organizations.

Data Availability

The data for this research can be downloaded from the link : https://physionet.org/content/chbmit/1.0.0/

Author Contribution

The raw data were preprocessed and de-noising by Ghansyamkumar along with working on development of the topomaps, feature extractions from the images for training the ML models. The feature selection, generation of synthetic data and machine learning model performance checking was done by Dr. Hardik.

Declarations

Ethical Approval

This study is based on the publicly available EEG datasets provided by CHB-MIT. The same dataset can be downloaded from PhysioNet. The ethical approval is not needed because of preapproval process done by the data provider.

Consent for Publication Participants.

Consent was taken from the data collecting authority that is mentioned in the ethical approval.

Competing Interests

There is no any competing interests by the authors.

References

[1] Benzaid A, Djemili R, Arbateni K. Seizure detection using nonlinear measures over EEG frequency bands and deep learning classifiers. Computer Methods in Biomechanics and Biomedical Engineering. 2024;28(13):1-17. doi:10.1080/10255842.2024.2356634

[2] Bai L, Litscher G, Li X. Epileptic Seizure Detection Using Machine Learning: A Systematic Review and Meta-Analysis. Brain Sciences. 2025;15(6):634. doi:10.3390/brainsci15060634

Manuscript received 30 January 2026; Revised 20 March 2026; Accepted 2 April 2026; Available online 10 April 2026
Digital Object Identifier (**DOI**): https://doi.org/10.35882/jeeemi.v8i2.1515

[3] Tran LV, Tran HM, Le TM, Huynh TTM, Tran HT, Dao SVT. Application of Machine Learning in Epileptic Seizure Detection. Diagnostics. 2022;12(11):2879. doi:10.3390/diagnostics12112879

[4] Hassan F, Hussain SF, Qaisar SM. Epileptic Seizure Detection Using a Hybrid 1D CNN-Machine Learning Approach from EEG Data. Journal of Healthcare Engineering. 2022;2022:1-16. doi:10.1155/2022/9579422

[5] Zeng W, Shan L, Su B, Du S. Epileptic seizure detection with deep EEG features by convolutional neural network and shallow classifiers. Front Neurosci. 2023;17. doi:10.3389/fnins.2023.1145526

[6] Pekmezci M, Genc Y. Evaluation of SSIM loss function in RIR generator GANs. Digital Signal Processing. 2024;154:104685. doi:10.1016/j.dsp.2024.104685

[7] Sharma D. Image Quality Assessment Metrics for Hyperspectral Image Compression Algorithms. In: ; 2024:1-5. doi:10.1109/ic3tes62412.2024.10877577

[8] Habashi AG, Azab AM, Eldawlatly S, Aly GM. Generative adversarial networks in EEG analysis: an overview. J NeuroEngineering Rehabil. 2023;20(1). doi:10.1186/s12984-023-01169-w

[9] Bhat R, Nanjundegowda R. A Review on Comparative Analysis of Generative Adversarial Networks' Architectures and Applications. Journal of Robotics and Control. 2024;6(1):53-64. doi:10.18196/jrc.v6i1.24160

[10] Zhong L, Wan J, Wu J, et al. Temporal and spatial dynamic propagation of electroencephalogram by combining power spectral and synchronization in childhood absence epilepsy. Front Neuroinform. 2022;16(122). doi:10.3389/fninf.2022.962466

[11] Skaria S, Savithriamma SK. Automatic classification of seizure and seizure-free EEG signals based on phase space reconstruction features. J Biol Phys. 2024;50(2):181-196. doi:10.1007/s10867-024-09654-6

[12] Awais M, Belhaouari SB, Kassoul K. Graphical Insight: Revolutionizing Seizure Detection with EEG Representation. Biomedicines. 2024;12(6):1283. doi:10.3390/biomedicines12061283

[13] Deepa B, Ramesh K. Epileptic seizure detection using deep learning through min max scaler normalization. ijhs. Published online May 24, 2022:10981-10996. doi:10.53730/ijhs.v6ns1.7801

[14] Aslam MH, Usman SM, Khalid S, et al. Classification of EEG Signals for Prediction of Epileptic Seizures. Applied Sciences. 2022;12(14):7251. doi:10.3390/app12147251

[15] Kode H, Elleithy K, Almazaydeh L. Epileptic Seizure Detection in EEG Signals Using Machine Learning and Deep Learning Techniques. IEEE Access. 2024;12:80657-80668. doi:10.1109/access.2024.3409581

[16] Riccio C, Martone A, Zazzaro G, Pavone L. Training Datasets for Epilepsy Analysis: Preprocessing and Feature Extraction from Electroencephalography Time Series. Data. 2024;9(5):61. doi:10.3390/data9050061

[17] Prasanna J, Subathra MSP, Mohammed MA, Damaševičius R, Sairamya NJ, George ST. Automated Epileptic Seizure Detection in Pediatric Subjects of CHB-MIT EEG Database-A Survey. JPM. 2021;11(10):1028. doi:10.3390/jpm11101028

[18] Alturki FA, Aljalal M, Abdurraqeeb AM, Alsharabi K, Al-Shamma'A AA. Common Spatial Pattern Technique With EEG Signals for Diagnosis of Autism and Epilepsy Disorders. IEEE Access. 2021;9:24334-24349. doi:10.1109/access.2021.3056619

[19] Park B, Jeong C, Ok J, Kim TI. Materials and Structural Designs toward Motion Artifact-Free Bioelectronics. Chem Rev. 2024;124(10):6148-6197. doi:10.1021/acs.chemrev.3c00374

[20] Maddirala AK, Veluvolu KC. SSA with CWT and k-Means for Eye-Blink Artifact Removal from Single-Channel EEG Signals. Sensors. 2022;22(3):931. doi:10.3390/s22030931

[21] Dong L, Zhao L, Zhang Y, et al. Reference Electrode Standardization Interpolation Technique (RESIT): A Novel Interpolation Method for Scalp EEG. Brain Topogr. 2021;34(4):403-414. doi:10.1007/s10548-021-00844-2

[22] Hirata A, Niitsu M, Phang CR, et al. High-resolution EEG source localization in personalized segmentation-free head model with multi-dipole fitting. Phys Med Biol. 2024;69(5):055013. doi:10.1088/1361-6560/ad25c3

[23] Choi K, Chong K. Modified Inverse Distance Weighting Interpolation for Particulate Matter Estimation and Mapping. Atmosphere. 2022;13(5):846. doi:10.3390/atmos13050846

[24] Gong R, Roth RW, Chang AJ, et al. EEG Ictal Power Dynamics, Function-Structure Associations, and Epilepsy Surgical Outcomes. Neurology. 2024;102(12). doi:10.1212/wnl.0000000000209451

[25] Onakpojeruo EP, Mustapha MT, Ozsahin DU, Ozsahin I. A Comparative Analysis of the Novel Conditional Deep Convolutional Neural Network

Manuscript received 30 January 2026; Revised 20 March 2026; Accepted 2 April 2026; Available online 10 April 2026
Digital Object Identifier (**DOI**): https://doi.org/10.35882/jeeemi.v8i2.1515

Model, Using Conditional Deep Convolutional Generative Adversarial Network-Generated Synthetic and Augmented Brain Tumor Datasets for Image Classification. Brain Sciences. 2024;14(6):559. doi:10.3390/brainsci14060559
[26] Zhang Z, Liu Y, Zhong SH. GANSER: A Self-Supervised Data Augmentation Framework for EEG-Based Emotion Recognition. IEEE Trans Affective Comput. 2023;14(3):2048-2063. doi:10.1109/taffc.2022.3170369
[27] Gao M, Liu R, Mao J. Noise Robustness Low-Rank Learning Algorithm for Electroencephalogram Signal Classification. Front Neurosci. 2021;15. doi:10.3389/fnins.2021.797378
[28] Sara U, Akter M, Uddin MS. Image Quality Assessment through FSIM, SSIM, MSE and PSNR—A Comparative Study. JCC. 2019;07(03):8-18. doi:10.4236/jcc.2019.73002
[29] Aayesha A, Qureshi MB, Afzaal M, Qureshi MS, Fayaz M. Machine learning-based EEG signals classification model for epileptic seizure detection. Multimed Tools Appl. 2021;80(12):17849-17877. doi:10.1007/s11042-021-10597-6
[30] Nti IK, Nyarko-Boateng O, Aning J. Performance of Machine Learning Algorithms with Different K Values in K-fold CrossValidation. IJITCS. 2021;13(6):61-71. doi:10.5815/ijitcs.2021.06.05
[31] Rimal Y, Sharma N, Paudel S, Alsadoon A, Koirala MP, Gill S. Comparative analysis of heart disease prediction using logistic regression, SVM, KNN, and random forest with cross-validation for improved accuracy. Sci Rep. 2025;15(1). doi:10.1038/s41598-025-93675-1
[32] Ayman U, Zia MS, Okon OD, et al. Epileptic Patient Activity Recognition System Using Extreme Learning Machine Method. Biomedicines. 2023;11(3):816. doi:10.3390/biomedicines11030816
[33] Janiukstyte V, Owen TW, Chaudhary UJ, et al. Normative brain mapping using scalp EEG and potential clinical application. Sci Rep. 2023;13(1). doi:10.1038/s41598-023-39700-7
[34] Zhang S, Liu P, Mao X, Sun L. EEG topomap-based Identification scheme. In: ; 2021:287-293. doi:10.1109/iaecst54258.2021.9695816
[35] Nilsson J, Akenine-Möller T. Understanding SSIM. Published online June 24, 2020. doi:10.48550/arxiv.2006.13846
[36] Reznik Y. Another look at SSIM image quality metric. ei. 2023;35(8):305-7. doi:10.2352/ei.2023.35.8.iqsp-305
[37] Zhang S, Sun L, Mao X, Yang Y. EEG data augmentation for Personal Identification Using SF-GAN. In: ; 2022:1-6. doi:10.1109/cvidliccea56201.2022.9824276
[38] Wang Z, Liu F, Shi S, et al. Automatic epileptic seizure detection based on persistent homology. Front Physiol. 2023;14(12). doi:10.3389/fphys.2023.1227952
[39] Chung YG, Cho A, Kim H, Kim KJ. Single-channel seizure detection with clinical confirmation of seizure locations using CHB-MIT dataset. Front Neurol. 2024;15. doi:10.3389/fneur.2024.1389731
[40] Shen M, Yang F, Wen P, Song B, Li Y. A real-time epilepsy seizure detection approach based on EEG using short-time Fourier transform and Google-Net convolutional neural network. Heliyon. 2024;10(11):e31827. doi:10.1016/j.heliyon.2024.e31827
[41] Ali E, Angelova M, Karmakar C. Epileptic seizure detection using CHB-MIT dataset: The overlooked perspectives. R Soc Open Sci. 2024;11(5). doi:10.1098/rsos.230601
[42] Abou-Abbas L, Henni K, Jemal I, Mezghani N. Generative AI with WGAN-GP for boosting seizure detection accuracy. Front Artif Intell. 2024;7. doi:10.3389/frai.2024.1437315
[43] Zhu R, Pan WX, Liu JX, Shang JL. Epileptic seizure prediction via multidimensional transformer and recurrent neural network fusion. J Transl Med. 2024;22(1). doi:10.1186/s12967-024-05678-7

Author Biography

Ghansyamkumar Rathod was graduated in 2007 with Bachelor of Engineering (B.E) in Electronics from Birla Vishvakarma Mahavidyalaya (BVM) affiliated with Sardar Patel University (SPU) and Master of Engineering (M.E) in Communication from G.H.Patel college of Engineering and technology (GCET) Gujarat Technological University (GTU) in 2012. He is doing part time Ph.D from Charotar University of Science and Technology (CHARUSAT). Along with teaching experience of more than 17 years, he is also having keen interest in Biomedical signal processing, sensors and transducers, robotics technology, circuits and networks, simulation and interfacing and analog electronics. He had supervised more than 30 mini and Major Electronics projects at UG and PG level. https://orcid.org/0000-0001-9613-2988

Manuscript received 30 January 2026; Revised 20 March 2026; Accepted 2 April 2026; Available online 10 April 2026
Digital Object Identifier (**DOI**): https://doi.org/10.35882/jeeemi.v8i2.1515

Dr. Hardik Modi was graduated in 2005 with Bachelor degree in Electronics and Communication Engineering from A.D Patel Institute of Technology (ADIT) under Sardar Patel University (SPU). He did Master of Engineering in Communication system from Dharmsinh Desai University (DDU) in 2007 and Doctorate of Philosophy from Charotar University of Science and Technology (CHARUSAT) in 2016. He serving as an Associate professor at CSPIT. He is having teaching experience of more than 19 years. His field of interest is in single processing, VLSI and Embedded system design, circuit and networks. He had guided many UG, PG and PhD students. https://orcid.org/0000-0002-1847-4234

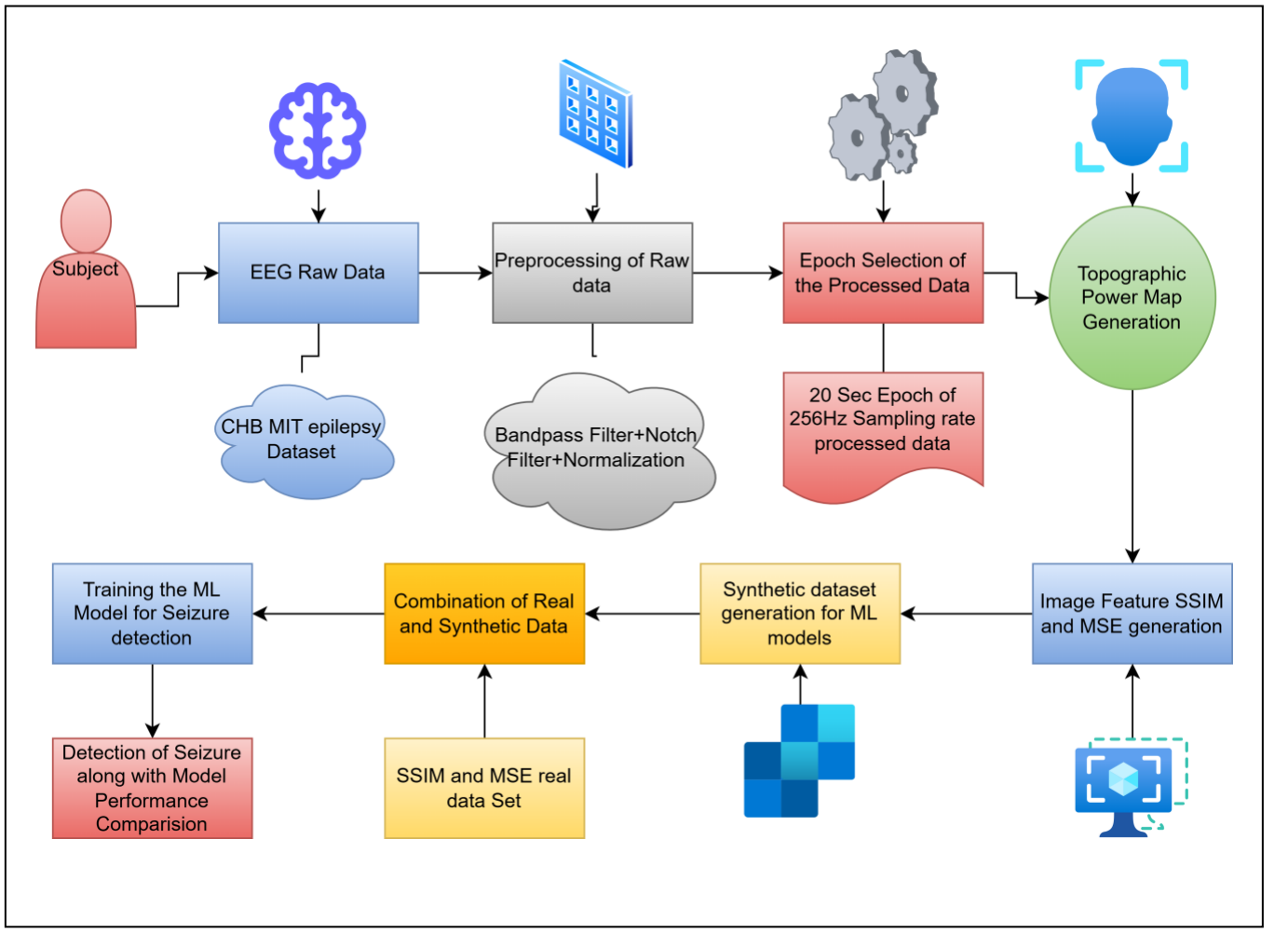

Manuscript received 30 January 2026; Revised 20 March 2026; Accepted 2 April 2026; Available online 10 April 2026
Digital Object Identifier (**DOI**): https://doi.org/10.35882/jeeemi.v8i2.1515